JOURNAL OF GEOPHYSICAL RESEARCH, VOL. 115, A06105, doi:10.1029/2009JA014841, 2010

One-dimensional electromagnetic simulation of multiple electron beams propagating in space plasmas

F. J. R. Simões Jr.,[1,2] M. V. Alves,[1] and R. Gaelzer[3]

Received 31 August 2009; revised 4 December 2009; accepted 6 January 2010; published 18 June 2010.

[1] It is by now well known that electron beams play an important role in generating radio emissions such as type II and type III radio bursts, commonly observed by spacecraft in the interplanetary medium. Electron beams streaming back from Earth's bow shock into the solar wind have been proposed as a possible source for the electron plasma waves observed by spacecraft in the electron foreshock. Recent observations suggest that during the natural evolution of the foreshock plasma, multiple electron beams could be injected over a period of time, losing their individual identity to coalesce into a single beam. In this work, we use an electromagnetic particle-in-cell (PIC) code "KEMPO 1D, adapted" to simulate two electron beams that are injected into a plasma at different times. The first beam disturbs the background plasma and generates Langmuir waves by electron beam-plasma interaction. Subsequently, another beam is inserted into the system and interacts with the first one and with the driven Langmuir waves to produce electromagnetic radiation. The results of our simulation show that the first beam can produce electrostatic harmonics of the plasma frequency, while the second beam intensifies the emission at the harmonics that is produced by the first one. The behavior of the second beam is strongly determined by the preexisting Langmuir wave electric fields. The simulations also show, as a result of the interaction between both beams, a clear nonlinear frequency shift of the harmonic modes as well as an increase of electromagnetic and kinetic energies of the wave-particle system.

Citation: Simões, F. J. R., Jr., M. V. Alves, and R. Gaelzer (2010), One-dimensional electromagnetic simulation of multiple electron beams propagating in space plasmas, *J. Geophys. Res.*, *115*, A06105, doi:10.1029/2009JA014841.

1. Introduction

[2] Electron beams propagating away from the Sun play an important role in generating solar radio emissions and are basic phenomena observed on solar activities. When a solar flare occurs, electron beams are injected from the Sun into the interplanetary medium. These electron beams propagate along the interplanetary magnetic field lines with velocities parallel to the magnetic field that are much larger than the electron thermal speed of the solar wind. Near Earth's magnetosphere, electrons are streaming back from the shock into the solar wind, driving Langmuir waves through beam-plasma or bump-on-tail instabilities [*Canu*, 1989]. Subsequently, the Langmuir waves can be converted to electromagnetic radiation either at the fundamental, $f = f_p$, or at the first harmonic, $f = 2f_p$, or both.

[3] A theoretical picture of type II and type III solar radio bursts and $2f_p$ radiation from the terrestrial electron foreshock was first proposed by *Ginzburg and Zheleznyakov* [1958]. The core of this picture is still used today: in the source region, Langmuir waves are generated by a bump-on-tail instability of electron beams. The bump-on-tail instability involves only those particles that are in resonance with the wave. Particles with velocities greater than wave phase velocity contribute to the growth of the wave; those with velocities smaller than phase velocity contribute to the damping [*Gurnett and Bhattacharjee*, 2004]. Growth of Langmuir waves then tends to relax the beam to prevent marginal stability by quasi-linearly flattening its velocity distribution.

[4] With the technological development of the last few decades, computer experiments have been increasingly employed to understand the physical processes of space plasmas [*Matsumoto and Sato*, 1985; *Birdsall and Langdon*, 1991; *Omura and Matsumoto*, 1993; *Birdsall and Fuss*, 1997; *Umeda et al.*, 2003]. An intriguing feature in electrostatic simulations, Vlasov and particle-in-cell (PIC), of beam-plasma interactions is the ubiquitous excitation of harmonic electrostatic modes, $2\omega_{pe}$, and even higher harmonics, $3\omega_{pe}$ and $4\omega_{pe}$, for example, with decreasing intensities for increasing harmonics. Recent theories in the literature [*Umeda et al.*, 2003; *Yoon*, 2000; *Yoon et al.*, 2003; *Gaelzer*

[1]Laboratório Associado de Plasmas, Instituto Nacional de Pesquisas Espaciais, São José dos Campos, Brazil.
[2]Now at Instituto de Física e Matemática, Universidade Federal de Pelotas, Pelotas, Brazil.
[3]Instituto de Física e Matemática, Universidade Federal de Pelotas, Pelotas, Brazil.

0148-0227/10/2009JA014841

et al., 2003] for the harmonic generation consider the harmonics as nonlinear eigenmodes of a beam-plasma system. This approach was followed by simulations developed by *Kasaba et al.* [2001] and *Schriver et al.* [2000]. They show that harmonic modes persist even in the late nonlinear phase when the coherent phase space structure is no longer apparent and when the plasma has entered a stage which can be genuinely characterized by random phases.

[5] The simulations by *Schriver et al.* [2000] and *Kasaba et al.* [2001], which were designed to resolve only up to the first harmonic (that is, $n = 1$ and 2), clearly show, from the obtained ω-k diagram, that the first harmonic mode occupies a broad spectral range which can be best described by a phenomenological dispersion relation.

[6] In space plasmas, electron beams can assume the shape of more than one electron beam. They could be injected into the interplanetary medium where the local plasma is inhomogeneous with both regular monotonic spatial variations (for example, the r^{-2} falloff from the Sun) and irregular spatial variations (e.g., due to turbulence). On the basis of this possibility, recent research has adopted a more realistic condition, that is, including more than one electron beam to study the dynamics of the system, in order to understand the physical picture about electrostatic and electromagnetic emission [*Li et al.*, 2002].

[7] *Li et al.* [2002] investigated numerically the propagation of multiple electron beams using quasi-linear theory. They noticed that the mechanism of beam merging is via interaction between beam particles and associated waves. Fast particles in a trailing beam lose energy to waves generated previously by the leading beam, while slow particles in the leading beam absorb energy from waves driven by the trailing beam, which eventually leads to the elimination of any measurable speed difference between the two beams. These findings suggest that multiple electron beams could be injected over a period of time and they tend to lose their individual identity to form just a single beam.

[8] Motivated by these recent results, we examine the emission of plasma waves and its harmonics from multiple electron beams injected at different times via the PIC code (KEMPO 1D) [*Omura and Matsumoto*, 1993] in a modified version [*Simões Junior*, 2008]. We consider a simple environment in our model: at $t = 0$ the first beam is injected into the system which is let to evolve; after a certain time a second beam is injected with defined characteristics and the simulation continues. Both beams occupy all the system at the time of their injection. This procedure was chosen to avoid grid effects at the boundaries. The initial conditions for the background plasma and the electron beams are based on solar wind and electron foreshock observations [*Anderson et al.*, 1985]. It is important to mention that in our code three components of velocity, three components of current, and three components of electric field are considered. The 1-D simulation limits our code to two components of magnetic field and one space component. In this case, all possible processes of coalescence and electromagnetic emission are not reproduced. Nevertheless, we clearly observe the electromagnetic waves propagating in arbitrary directions in our simulations. Previous 2-D simulations [*Kasaba et al.*, 2001] indicate that the obtained electromagnetic wave does not have the power observed in the interplanetary medium. Our results suggest that a higher power can be obtained as a consequence of multiple electron beam interactions, as shown by the continuous growth of electromagnetic energy after the second beam injection in Figure 7. Some of the mechanisms responsible for electromagnetic emission have been extensively reviewed by *Li et al.* [2005a, 2005b].

[9] This paper is organized as follows: section 2 presents the main characteristics of the simulation model. In section 3 we present the simulation results; in section 4 we present a summary and the conclusions of our work.

2. Simulation Model

[10] The physical picture used in this paper is of a magnetized, background plasma interacting with electron beams, which are injected into the system in different times. Simulations are performed using a one-dimensional modified version of the electromagnetic particle code KEMPO (Kyoto Electromagnetic Particle Code) [*Omura and Matsumoto*, 1993] with periodic boundary conditions. The first beam, injected at $t = 0$, is responsible for breaking the equilibrium of the system, with the ensuing generation of Langmuir waves. The system is allowed to evolve for a certain period of time when a new starting condition is imposed. The original code was modified so that a second beam was injected, and the wave-particle system that resulted from the beam-plasma interaction during the previous run was employed as the new background system.

[11] For the numerical simulation we use 2048 spatial grids points, with distances normalized by λ_D, where $\lambda_D = (\varepsilon_0 K_B T_e / n_e e^2)^{1/2}$ is the Debye length, K_B is the Boltzmann constant, e is the elementary charge, and T_e and n_e are the electron temperature and equilibrium density, respectively. The grid spacing is $\Delta x = 1.0$. All frequencies are normalized by the electron plasma frequency $\omega_{pe} = (n_e e^2 / m_e \varepsilon_0)^{1/2}$, and all velocities are normalized by electron thermal velocities $v_{the} = (K_B T_e / m_e)^{1/2}$. The simulations run for a total of 16,384 time steps, with $\Delta t = 0.02\omega_{pe}^{-1}$. After injecting the first beam, the system is let to evolve until $\omega_{pe} t = 327.68$, which is equivalent to $\Omega_{ce} t = 163.84$, where $\Omega_{ce} = eB_0/m_e$ is the electron gyrofrequency, B_0 is the ambient magnetic field, and m_e is the electron rest mass. The electron drift velocities are $v_{de} = 0.1 v_{the}$ and $v_{db1} = 7.5 v_{the}$ for a standard run, where v_{de} and v_{db1} are the background electron plasma and first electron beam drift velocities, respectively. The ions are considered stationary and are only included for charge neutrality. We consider 512 superparticles by grid cell for the background plasma and 256 superparticles by grid cell for the first and second beams. The 1-D simulation limits our code to three components of velocity, current, and electric field; two components of magnetic field; and one space component.

[12] We consider that the background plasma and the first and second beams are described by isotropic Maxwellian distribution functions. Figure 1 shows the velocity distribution functions at $t = 0$ for the four cases that we will treat here. A solid line represents the background plasma, a line with asterisks represents the first electron beam, and a line with squares represents the second electron beam. We also assume that the two beams have the same characteristic

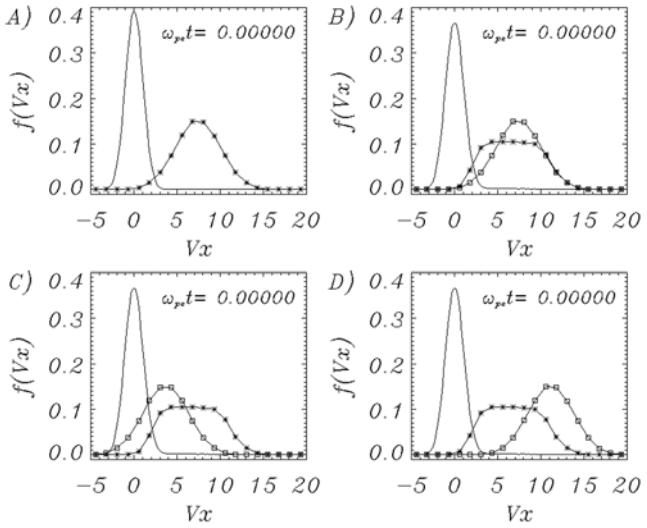

Figure 1. Schematic Maxwellian velocity distribution function for the four different cases considered. (a) A single electron beam with drift velocity injected into a ambient plasma, this case is performed to disturb the system and generate Langmuir waves. (b) A second electron beam with the same drift velocity of the first beam. (c) We consider that the second electron beam is slower than the first beam. (d) We assume that the second electron beam is faster than the first beam. Background plasma is represented by a solid line, the first electron beam is represented by a line with asterisks, and the second electron beam is represented by a line with squares.

plasma frequencies given by $\omega_{pb1,2} = 0.35\omega_{pe}$ and the same thermal velocities, equal to $2.54v_{the}$, for all simulation runs.

[13] The standard case (Figure 1a) is performed to disturb the system and generate Langmuir waves. Then we consider three additional cases, varying the drift velocity for the second beam. For the first case, we assume that the second beam has the same velocity as the first beam, $v_{db2\text{-}F} = 7.5v_{the}$ (Figure 1b); for the second case, we assume that the second beam is slower than the first, with $v_{db2\text{-}S} = 3.75v_{the}$ (Figure 1c); and for the third case, we consider a faster second beam with $v_{db2\text{-}T} = 11.25v_{the}$ (Figure 1d). The subindexes *db2-F*, *db2-S* and *db2-T* denote the drift velocities of the second beam for the first, second, and third cases, respectively.

[14] Note the plateau formation in the first electron beam distribution function, which is a consequence of the beam-plasma interaction [*Melrose*, 1986], for the first, second, and third cases. At $t = 0$, we consider that the first beam has been fully injected into the system; that is, the electron beam is not injected into the system, it occupies all the system at $t = 0$. This procedure avoids grid effects at the boundaries. For all cases, before the second beam is injected, a standard run, with only the background plasma and the first beam, is performed for a certain amount of time. The system is allowed to nonlinearly evolve from the equilibrium situation during this period until the beam plasma instability saturates. At this point the run is interrupted, and all information necessary to restart the run is saved. The resulting system is then used as the new background system, the second beam is injected, and the simulation is resumed.

3. Simulation Results

[15] In this section we present results for the four different simulation runs described in section 2.

3.1. Standard Case

[16] The most important emission mechanism for meter wave solar bursts is "plasma emission. " In general, at least three stages are involved. The first stage is the generation of Langmuir turbulence. The second and third stages involve nonlinear plasma processes which convert the energy in the Langmuir turbulence in escaping transverse waves at the fundamental and harmonics of plasma frequency. Our standard case represents the first stage and is used as a first step to reach the other two. In this case, we inject a single beam into the background plasma, considering the beam density as approximately 12% of the background plasma density.

[17] Figure 2 shows the time evolution of the total electric field energy, W_E, total magnetic field energy, W_B, and the kinetic and the total energies of the system for the standard case. In all results presented here, energy is measured in arbitrary units. At $\omega_{pe}t = 0.0$ one can see that W_E is zero (Figure 2, top left). It is important to mention that there are no waves in the system at this instant. They will be generated during the simulations.

[18] Comparing all frames of Figure 2, we can see that W_E grows at the expense of the kinetic energy, K_E (Figure 2, bottom left), reaching a maximum of 0.09 (arbitrary units). Changes in W_B are negligible compared to the variations of W_E. Although not shown here, W_E is mainly determined by the parallel component of the electric field (Langmuir waves). The total energy (Figure 2, bottom right), the sum of kinetic, magnetic, and electric field energies, is conserved.

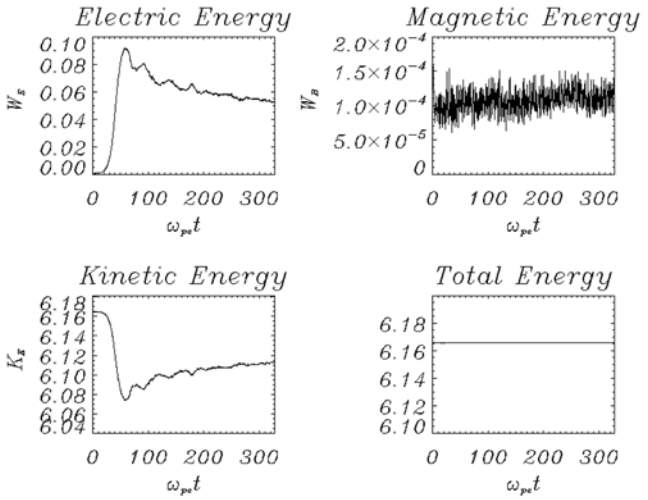

Figure 2. Time evolution of (top left) total electric field energy, W_E, (top right) total magnetic field energy, W_B, (bottom left) kinetic energy, K_E, and (bottom right) the total system energy (electric plus magnetic plus kinetic energy) for the standard case for only the single electron beam injected into the background plasma.

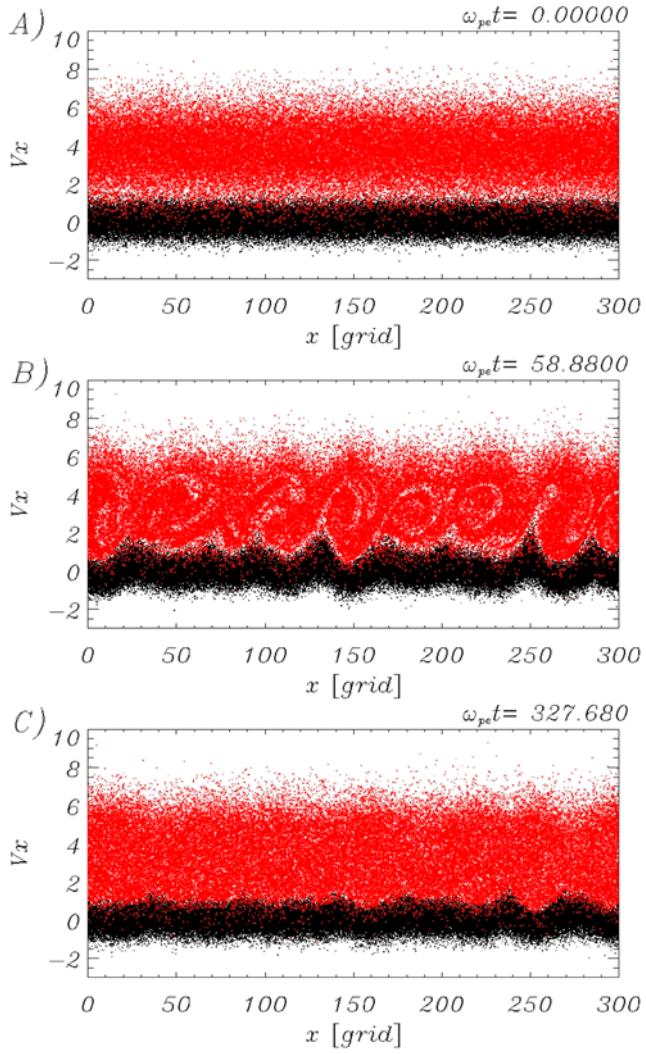

Figure 3. Phase space diagrams, v_x versus x, at different times along the simulation. Background plasmas are black, and first electron beams are red.

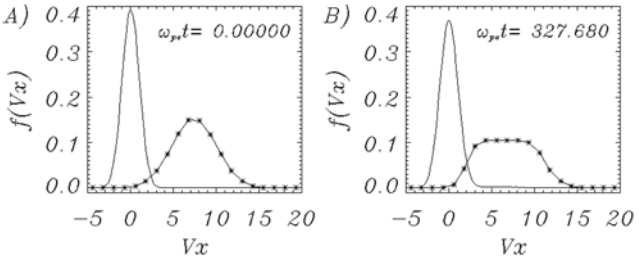

Figure 4. Velocity distribution function for the standard case. (a) Initial time and (b) final time of the simulation are presented. The solid line shows the background plasma, and the line with asterisks shows the first beam.

This is evidence that numerical instabilities are absent in our simulations. All the results presented here are characterized by the same numerical stability, and thus, we will not present further time evolution results for the total energy of the wave-particle system.

[19] The plot for W_E in Figure 2 (top left) shows that there are three peaks: the first one at $\omega_{pe}t$ = 58.88, the second at $\omega_{pe}t$ = 94.7, and the third at $\omega_{pe}t$ = 138.2. The first peak marks the end of the quasi-linear growth process, started with the linear growth rate $\gamma_{WE} = 0.134\omega_{pe}^{-1}t^{-1}$. During this stage, the Langmuir wave generation is associated with vortex formation in the electron velocity phase space.

[20] Figure 2 shows that the first beam plasma instability saturates at $W_E \approx 0.05$, in agreement with theoretical estimate [*Sotnikov et al.*, 1994]. The saturation instability is reached together with the plateau formation in the velocity distribution function. The growth of the velocity spread can stabilize the instability. This happens when damping produced by the beam electrons due to the velocity spread exceeds the growth rate connected with the resonant interaction with the background electrons [*Sotnikov et al.*, 1994].

[21] Figure 3 shows the phase space for particles at three different instants. Figure 3a shows the phase space at t = 0, Figure 3b shows it at $\omega_{pe}t$ = 58.88 (first W_E peak, the end of the quasi-linear stage), and Figure 3c shows it at the end of the simulation run, $\omega_{pe}t$ = 327.68. The background plasma is represented by black, and the first beam is shown in red.

[22] The basic time evolution of the velocity distribution function is presented in Figure 4. The background plasma is represented by a solid line, and the first beam is represented by the line with asterisks. At $\omega_{pe}t$ = 0.0 (Figure 4a) the first beam (for the standard case) is fully injected into the system. At the initial stage ($\omega_{pe}t$ = 0.0 → ≈58.88) the vortices are formed in the phase space, and after that, they are gradually disordered. Figure 4b, at $\omega_{pe}t$ = 58.88, presents a snapshot of when the first peak in W_E occurs (maximum electric field energy). At this time one can see that the beam distribution function is completely flattened. After this time, no important changes occur. A well-known plateau formation can be seen in Figure 4b at the final time of simulation.

[23] For the first stage of the simulation (one beam), further evolution of the velocity distribution function occurs on a timescale of the order of thousands of plasma periods. However, such long-time features are not of interest in the

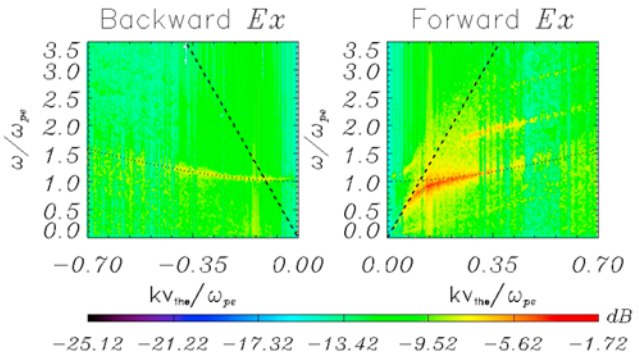

Figure 5. The ω-k diagram obtained from the time and space evolution of the x component of the electric field, E_x, along the ambient magnetic field. Total time of simulation is considered. The theoretical Bohm-Gross relation is shown by a dotted line, and tje beam mode dispersion relation is shown by a dashed line.

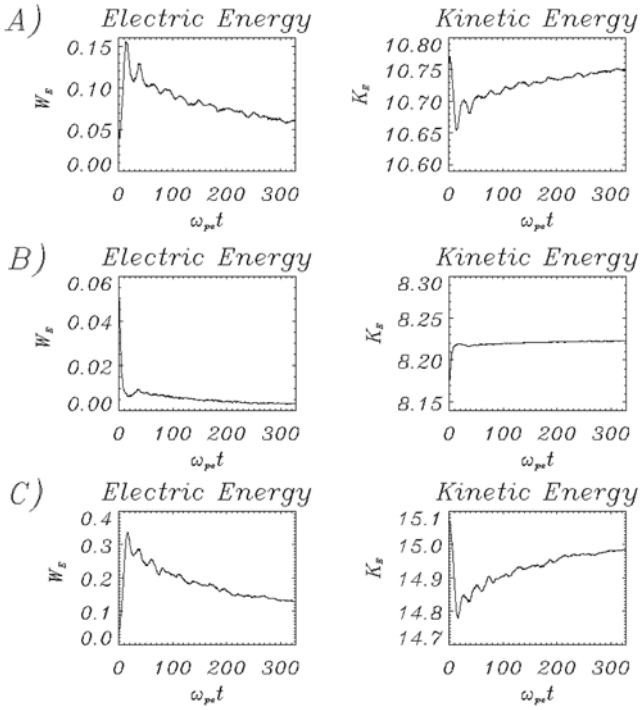

Figure 6. Time evolution of the (left) total electric field energy, W_E, and (right) kinetic energy, K_E. The second beam is injected into a perturbed plasma with three different drift velocities: (a) $v_{db2\text{-}F} = v_{db1}$, (b) $v_{db2\text{-}S} = 0.5v_{db1}$, and (c) $v_{db2\text{-}T} = 1.5v_{db1}$.

present study, because the ensuing injection of the second electronic beam will introduce a perturbation in the system that is characterized by a much shorter timescale.

[24] Figure 5 shows the ω-k diagram obtained from the x component of the electric field, E_x, along the ambient magnetic field by Fourier transforming in space along the x axis and in time. For reference, we also plot some theoretical plasma dispersion relations. The dotted line is the theoretical Bohm-Gross dispersion relation, $\omega^2 = \omega_{pe}^2 + 3v_{the}^2k^2$; the dashed line is the beam mode wave, $\omega = v_{db}k$.

[25] Figure 5 shows the excited Langmuir waves, at $\omega \lessapprox \omega_{pe} \approx 1.0$ for $k_x > 0$ (forward propagation). Initially, the wave number of the excited wave is lower than the expected value for the maximum linear growth rate, $k_x \sim \omega_{pe}/v_b = 0.13$. After the linear growth stage (vortex formation), the corresponding wave numbers become larger [*Dum*, 1990a, 1990b; *Nishikawa and Cairns*, 1991; *Kasaba et al.*, 2001]. Using the physical parameters of the standard case, we observe that $P = (\omega_{pb1}/\omega_{pe})^{2/3}(v_{db1}/v_{the1}) \approx 1.47$, where P is the parameter defined by *Cairns* [1989]. The dispersive characteristic and the emission spectrum of the fundamental mode are observed to closely follow the modified beam mode discussed by *Cairns* [1989]. The backward propagating ($k_x < 0$) Langmuir wave can also be seen in Figure 5 (left). Figure 5 also shows the presence of the harmonics for the forward propagation. The harmonics are generated during the linear growth stage and intensified after that. *Yoon et al.* [2003] developed a general theory for multiple harmonic generation and proposed that electrostatic harmonic waves are generated during the linear phase of the wave-particle interaction, as nonlinear eigenmodes of the beam-plasma system. This theory proposes that the harmonics are emitted around the intersection between the beam mode line and harmonic eigenmode dispersion relations [see, e.g., *Yoon et al.*, 2003, Figure 4]. Our results are in agreement with the theory formulated by *Yoon et al.* [2003].

[26] For a single beam, the standard case, our results present same qualitative behavior of previous PIC-1D simulations [*Kasaba et al.*, 2001; *Nishikawa and Cairns*, 1991; *Dum*, 1990a, 1990b]. However, none of the previous studies includes a second beam in the system disturbed by the first one.

3.2. Simulations With a Second Electron Beam

[27] In this section we present the results obtained by the injection of a second electron beam in the system previously perturbed by the first beam. We perform three simulation runs with the second electron beam. As the first case, we consider the second beam as having the same drift velocity as the first one, $v_{db2\text{-}F} = v_{db1}$; as the second case, we consider the second beam with the drift velocity given by $v_{db2\text{-}S} = 0.5v_{db1}$; and as the third case, we consider the second beam with $v_{db2\text{-}T} = 1.5v_{db1}$. All other simulation parameters are the same as in the standard case.

[28] Figure 6 presents the time evolution for the total electric field energy, W_E, and the kinetic energy, K_E, for the first case (Figure 6a), the second case (Figure 6b), and the third case (Figure 6c). Note that the initial value of W_E is not zero for these cases because of the presence of Langmuir waves driven by the first beam that produce a strong electric field, which interacts with the second electron beam. The resulting fast modulation of the second beam is characterized by a faster growth of W_E as compared to the standard case. In Figure 6a the peak is reached at $\omega_{pe}t \approx 12.8$, while for the standard case, it was reached just at $\omega_{pe}t = 58.88$. The growth rate for W_E is $\gamma_{WE} = 0.104$.

[29] In Figure 6b one can see that W_E decreases while the kinetic energy increases during the simulation time. The particles are accelerated at the expense of wave energy. In Figure 6c we can see that W_E increases from $W_E \approx 0.04$ to $W_E \approx 0.34$ during 13.62 plasma periods, with a growth rate $\gamma_{WE} = 0.157$. This increase occurs because of the strong electric field of the Langmuir waves that were driven in the system by the first beam. After the first peak, the electric field energy gradually decreases until the end of simulation. For all cases the energy exchange between the waves (electric field energy) and particles (kinetic energy) is clear. Similar results were obtained by *Li et al.* [2002] for multiple beams.

[30] One important result presented in this paper is the time profile of the electromagnetic energy (Figure 7). After the second beam injection into the system, the electromagnetic energy components ($E_y^2 + E_z^2$) grow more than the standard case (Figure 7a). Figure 7b shows the results obtained when the second electron beam has the same drift velocity of the first one, $v_{db2\text{-}F} = v_{db1}$; Figure 7c shows $v_{db2\text{-}S} = 0.5\ v_{db1}$; and Figure 7d shows $v_{db2\text{-}T} = 1.5\ v_{db1}$.

[31] In Figure 7c, it is important to note that although the second beam has a drift velocity smaller than the first one and the electrostatic energy has been absorbed, the electromagnetic energy keeps growing during the whole simulation time, with a growth rate of $\gamma_{el} = 1.6 \times 10^{-3}$. This result is

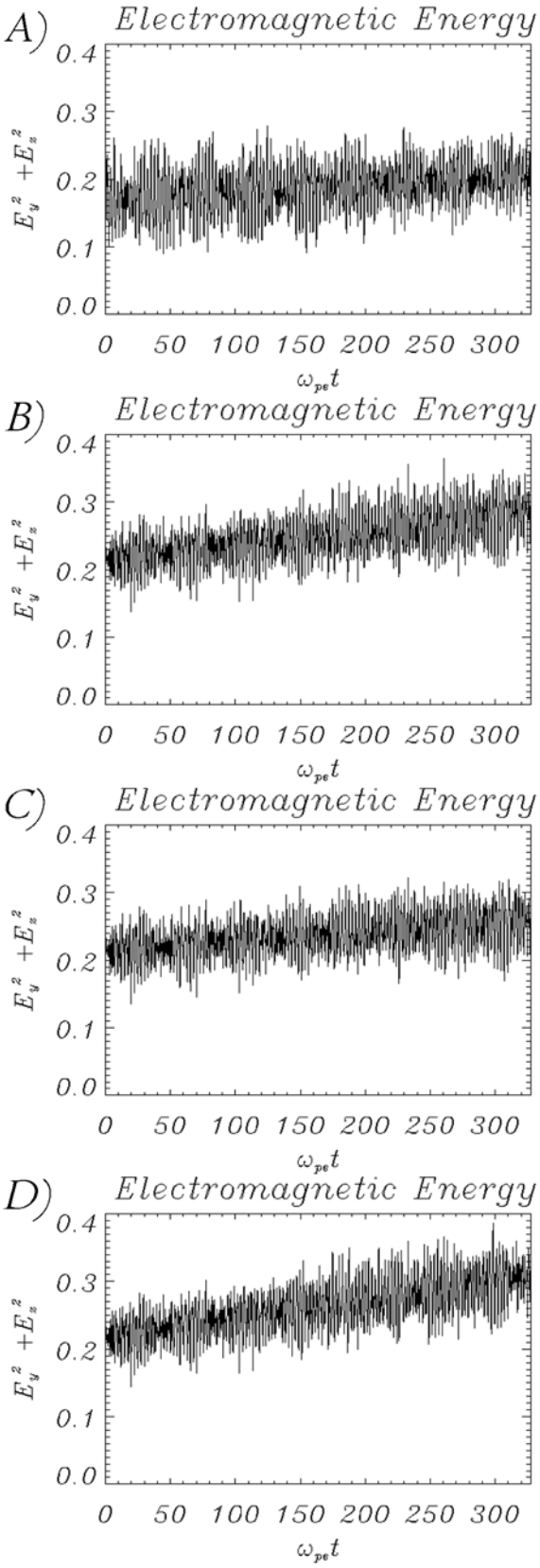

Figure 7. Time evolution of the electromagnetic field components energy ($E_y^2 + E_z^2$) during the whole simulation time after the injection of second electron beam: (a) standard case, (b) $v_{db2\text{-}F} = v_{db1}$, (c) $v_{db2\text{-}S} = 0.5v_{db1}$, and (d) $v_{db2\text{-}T} = 1.5v_{db1}$.

important because it suggests that multiple electron beams can be important in electromagnetic wave generation in space plasmas and solar bursts. However, this is an initial result that requires more systematic research in order to fully understand the electromagnetic wave generation processes. A 2-D code is being developed to address this subject.

[32] From Figure 7d we can see that when the second electron beam has a greater drift velocity than the first one, the electromagnetic energy grows more than in all the other cases. Although it is clear that the growth rate of the electromagnetic component of W_E is proportional to the amount of free energy pumped into the system by the second beam, the mechanism responsible for the energy transfer is not evident from the 1-D simulation results. We intend to pursue the subject further in future studies using a bidimensional PIC code.

[33] Figure 8 shows the ω-k diagram obtained from the time and space evolution of E_x, along the ambient magnetic field, for the total time of the simulation after injection of the second beam. We can observe in Figure 8a that the har-

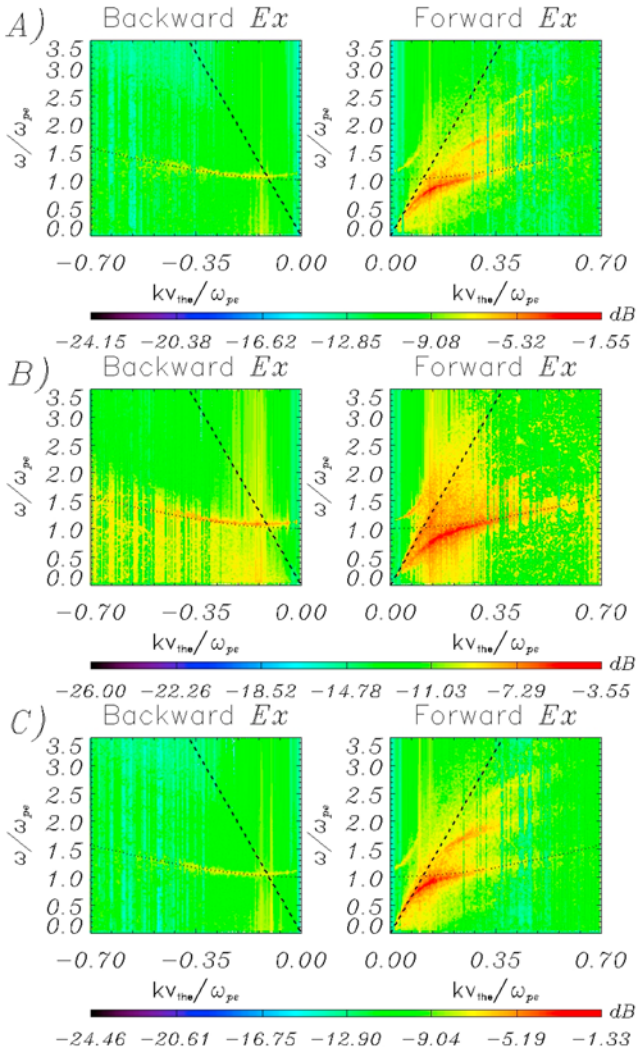

Figure 8. The ω-k diagram obtained by x component of the electric field, E_x, along the ambient magnetic field: (a) $v_{db2\text{-}F} = v_{db1}$, (b) $v_{db2\text{-}S} = 0.5v_{db1}$, and (c) $v_{db2\text{-}T} = 1.5v_{db1}$.

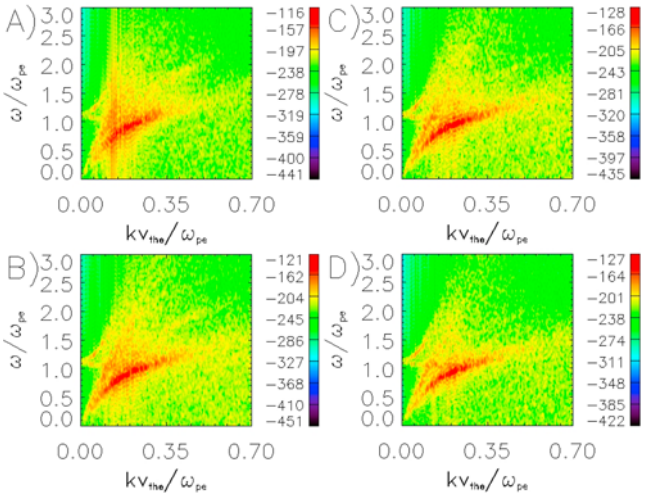

Figure 9. The ω-k diagrams for different intervals of time along the simulation for Figure 8b: (a) $\omega_{pe}t$ = 0–80, (b) $\omega_{pe}t$ = 80–160, (c) $\omega_{pe}t$ = 160–240, and (d) $\omega_{pe}t$ = 240–327, 68. We can see that harmonics are suppressed.

monic modes are downward shifted in frequency and they stand closer to one another than was observed in the standard case (Figure 5). For all cases with the second electron beam, the theoretical beam mode dispersion relation (dashed line) is obtained using the mean value of the sum of beam drift velocities, v_{db} = 7.5 (Figure 8a), v_{db} = 5.63 (Figure 8b), and v_{db} = 9.37 (Figure 8c).

[34] The relative intensities of the harmonic modes (Figures 8a and 8c) are also enhanced compared to the standard case, an effect that can be clearly noted on the first harmonic and that may be attributed to the excess of free energy as well. However, for $v_{db2} = (1/2)v_{db1}$ (Figure 8b), the harmonic emissions are largely suppressed, and the fundamental beam mode remains, with ≈10% of beam mode intensity compared to the standard case. This value is obtained from the comparative power spectrum, which is not show here.

[35] In an attempt to shed some light on the puzzling quenching of the harmonic emission, Figure 9 displays the $\omega \times k$ diagrams of four distinct time intervals, each one with 80 plasma cycles. At the beginning (Figures 9a and 9b), we can clearly see the first harmonic of plasma frequency ($\omega/\omega_{pe} \approx 1.5$). This harmonic is suppressed and disappears during the later 80 plasma cycles (Figures 9c and 9d). The fundamental mode energy is also partially absorbed.

[36] The behavior of the harmonic modes when $v_{db2} = (1/2)v_{db1}$ could be explained in terms of the linear Landau damping mechanism. Initially, Langmuir waves with phase velocity around v_{db1} are excited by the free energy provided by the first beam and grow to the levels displayed in Figure 5. Later, when the second beam is injected into the system with $v_{db2} < v_{db1}$, the particles at the leading edge of the beam, with $v \lessapprox v_{db1}$ and $\partial f_e/\partial v < 0$, start to tap into the energy provided by the preexisting Langmuir waves, thereby accelerating and damping the waves in the process. According to the theory of *Yoon et al.* [2003], the harmonic modes partake of the same linear induced absorption mechanism that affects the fundamental mode, being all absorbed or enhanced around the same beam line. Thus, since the harmonic modes intensities are comparatively lower than the fundamental, we can more easily observe those harmonics being damped back to the background radiation by the linear resonance with the second beam particles.

[37] Focusing our attention now on the third case ($v_{db2\text{-}T}$ = 1.5 v_{db1}), in Figure 8c we observe again the downward shifted and compacted harmonic modes, with a relatively less intense fundamental. In order to investigate the behavior of the harmonic modes in this case in greater detail, Figure 10 shows the ω-k diagrams for four distinct time intervals again, each one with 80 plasma cycles. We observe that the harmonics are present during the initial stage, $\omega_{pe}t = 0 \rightarrow 80$ (Figure 10a), reminding us of the standard case. However, at later times, they just kept growing (Figures 10b–10d), in a pattern that is the opposite of the second case.

[38] This behavior could also be explained in terms of the same mechanism that dampens the harmonic emission in the Figure 8b. In the present case, the electrons in the second beam, which now has $v_{db2} > v_{db1}$, start to resonate with the waves whose phase velocities are in the population inversion region of the second beam and that were previously excited by the first beam, thereby growing to higher levels. The frequency shift and the bunching of the harmonics would be due to nonlinear effects that are triggered by the enhanced level of the waves. Finally, in Figure 8 we can also clearly see the backscattered Langmuir mode with $k_x < 0$, which in all cases, closely follows the Bohm-Gross dispersion relation.

[39] The results presented in Figures 8–10 show an unmistakable frequency shift of the harmonic modes that requires further explanation. Although the nonlinear frequency shift of plasma eigenmodes due to the presence of weak or strong turbulence is a known phenomenon (see, e.g., the discussion by *Yoon and Gaelzer* [2002a, 2002b, and references therein]), it is usually only discussed in relation to the usual linear electrostatic eigenmodes (Langmuir and ion sound).

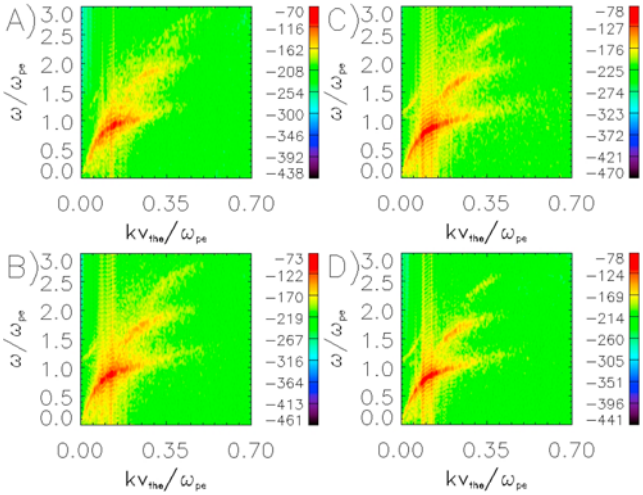

Figure 10. The ω-k diagrams for different intervals of time along the simulation for Figure 8c: (a) $\omega_{pe}t$ = 0–80, (b) $\omega_{pe}t$ = 80–160, (c) $\omega_{pe}t$ = 160–240, (d) $\omega_{pe}t$ = 240–327, 68. An intensification of harmonic emission is observed.

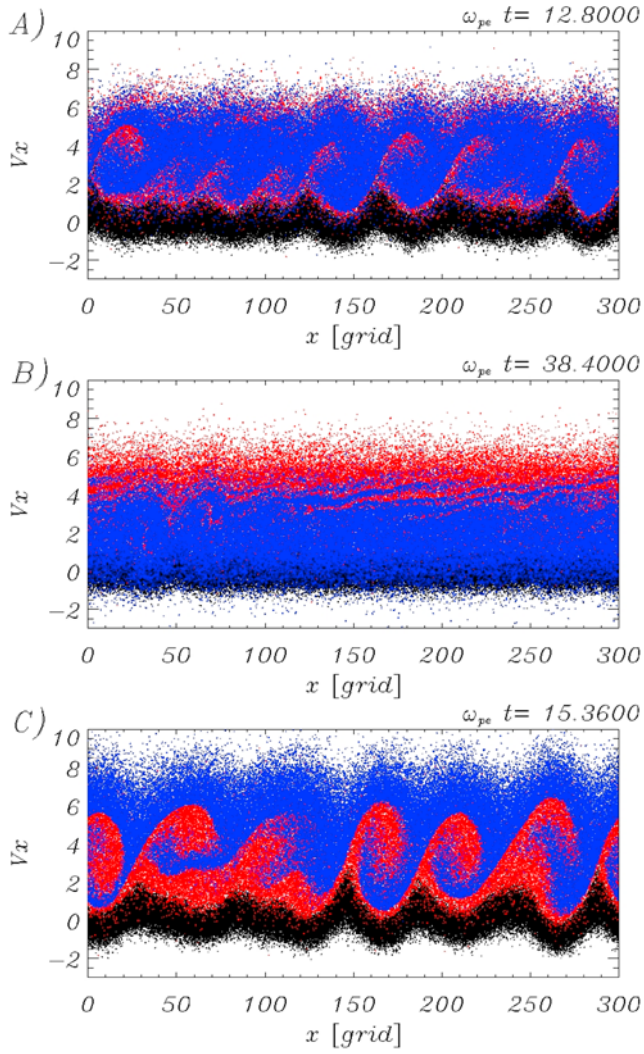

Figure 11. Phase space diagrams, v_x versus x, for the instant of time when W_E is at its maximum (Figure 6) for three different cases: (a) $v_{db2\text{-}T} = v_{db1}$, (b) $v_{db2\text{-}S} = 0.5v_{db1}$, and (c) $v_{db2\text{-}T} = 1.5v_{db1}$.

[40] The results presented in Figures 8–10 show that the frequency shift operates on the nonlinear harmonic modes as well, both by reducing the overall frequency of each harmonic and by reducing the frequency difference between two consecutive modes. In addition to the frequency shift, the relative intensity of the harmonic modes depends on the second beam drift speed and density in a complex manner that is not given by a simple proportional law. These effects, as far as we know, have not been identified by other simulation studies and require further simulation studies, which we intend to pursue in the future along with a theoretical explanation.

[41] In Figure 11 we can see that the second beam is quickly modulated by the strong electric field of the Langmuir waves. For the first case, $v_{db2\text{-}F} = v_{db1}$, the vortexes are present during the interval $\omega_{pe}t$ = 3–13. Figure 11a shows a snapshot of the first case at $\omega_{pe}t$ = 12.8, the same time when the peak W_E occurs (see Figure 6a). After this time, the system rapidly goes to a turbulent state, and the vortices are gradually destructed. At the end of the simulation the second electron beam is fully thermalized with the first one, and the system goes to equilibrium stage.

[42] After the injection of the second electron beam with lower drift speed (Figure 11b), the particles are quickly accelerated by the strong electric field of the Langmuir waves. The acceleration process occurs during the vortex formation, until $\omega_{pe}t$ = 10.24. This result can be confirmed by a fast energy exchange between the kinetic and electrical energy in Figure 6b, which occurs after this initial stage and continues until the end of simulation. In this case, the simulation time is not sufficient to complete plateau formation for the second beam, as seen in Figure 12.

[43] In the energy plot presented in Figure 6b, we can see a small increase in W_E between $\omega_{pe}t \approx 10.24$ and ≈ 38.4. Figure 11b shows that the peak in W_E is related to a new vortex formation between the first (red) and second (blue) beams. We believe that this new unstable stage contributes for particle acceleration of second beam. That period of time is related to a quick change in the shape of velocity distribution function for the second beam (blue in Figure 11) observed in Figure 12 from $\omega_{pe}t$ = 10.24 to 48.64. We can also observe the formation of a high-velocity "hump" on the second beam distribution around $v_x \approx 6$, indicating the acceleration of those particles by the electric field generated inside the vortices.

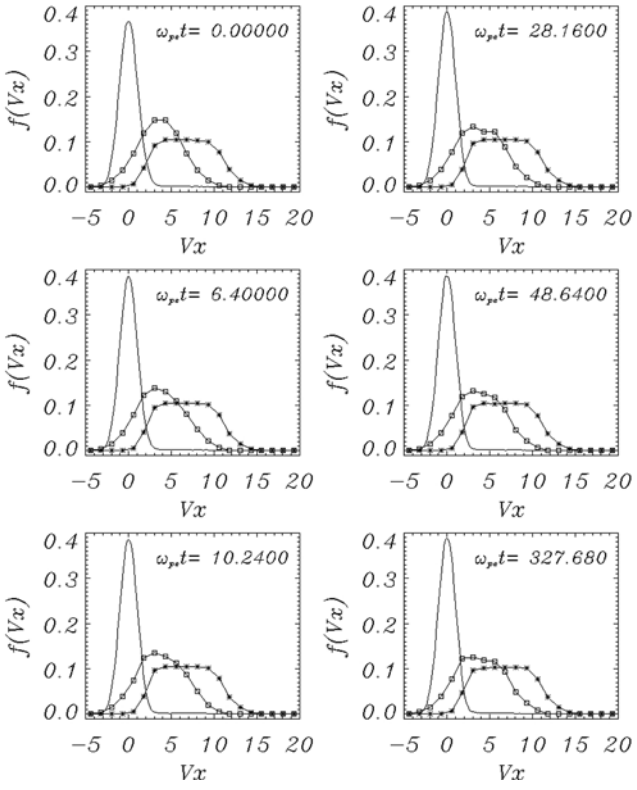

Figure 12. Velocity distribution function for the second case, $v_{db2\text{-}S} = 0.5v_{db1}$. Different times along the simulation are presented. The line with asterisks shows the first beam, and the line with squares shows the second beam.

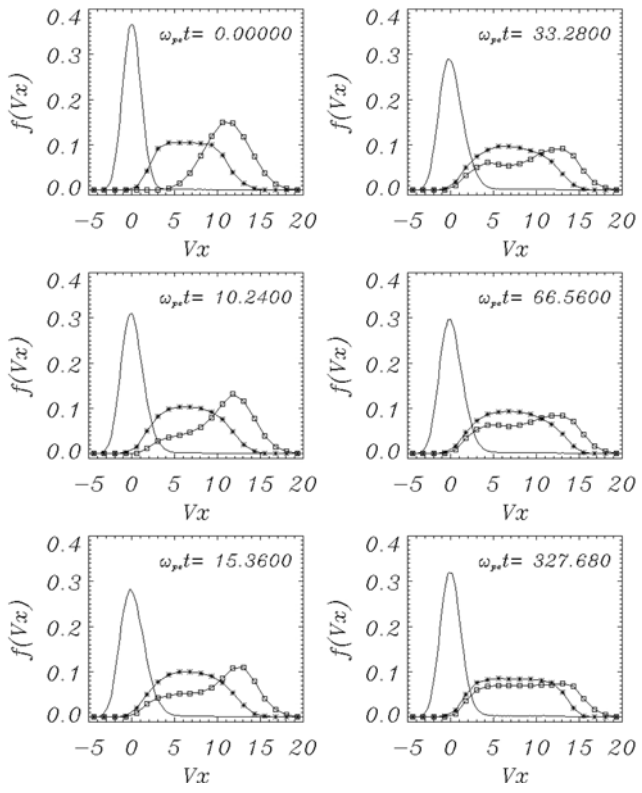

Figure 13. Velocity distribution function for the third case, $v_{db2\text{-}T} = 1.5v_{db1}$. Different times along the simulation are presented. The line with asterisks shows the first beam, and the line with squares shows the second beam.

[44] For the third case, $v_{db2\text{-}T} = 1.5v_{db1}$, the results shown in Figure 11c present the same qualitative behavior as the first case, i.e., the beam is quickly modulated by the strong electric field of the Langmuir waves. In the initial time of the simulation the vortices that are generated are even more prominent than in the first case and, again, are gradually disordered during the simulation. In that case, we can see that fast particles of the second electron beam transfer energy to slow particles of the first electron beam. These results are in agreement with a previous theoretical study that considered multiple beam emissions [*Li et al.*, 2002].

[45] For the third case, in the velocity distribution function plots presented in Figure 13, we can see that the shape of velocity distribution function for the first beam (line with asterisks) is strongly modified by the second beam (line with squares). After the inclusion of the second beam, the plateau that was formed in the first beam is destroyed, temporarily assuming a new Gaussian profile at $\omega_{pe}t = 10.24$. The slow particles of the first beam are accelerated by the fast particles of the second beam. At $\omega_{pe}t = 33.28$ we can see the formation of a new peak in the velocity distribution function for the second beam (line with squares) in $v_x \approx 4.0$. That concentration of slow particles in the second beam produces a deceleration of those particles of the first beam (line with asterisks) that have velocity greater than $v_x \approx 4.0$. A new diffusion process then ensues, where the temporary Gaussian profile of the first beam particles is changed into a new plateau, although with a slightly larger velocity spread than the original one (compare snapshots at $\omega_{pe}t = 0.0$ and $\omega_{pe}t = 327.68$).

[46] As in the first case, the nonlinear wave-particle interactions gradually remove the differences in drift velocities and shape of both beams, rendering both indistinguishable at the end of the simulation run. We believe that the same would be true for the second case, had we run the simulation for a longer time.

4. Summary

[47] Radio observations provide valuable tools for studying the solar drivers of space weather. In particular, they are associated with coronal and interplanetary (IP) shocks, energetic particles, and transient disturbances of IP medium. All these phenomena are potentially geoeffective and involve electromagnetic radiation emission by multiple beams of energetic particles. In this paper we have examined the plasma emissions resulting from a multiple electron beam plasma interaction by performing a computer experiment using a PIC simulation model (KEMPO 1D, adapted).

[48] The importance of the present paper lies in understanding the influence of a second electron beam injection in plasma frequency harmonic generation. Results obtained for the standard case, a single beam, show that backward propagating electrostatic Langmuir waves appear at $k_x < 0$ (see Figure 5). We believe that these waves are resulting from the forward excited Langmuir wave decay, as predicted by nonlinear theory [*Zakharov*, 1984; *Robinson*, 1997; *Alves et al.*, 2002; *Simões Junior et al.*, 2005] and observed in previous simulations [*Kasaba et al.*, 2001; *Nishikawa and Cairns*, 1991]. Harmonic emissions of the fundamental forward propagating electrostatic beam mode are also clearly seen at a somewhat later time in the simulation, although still within the quasi-linear stage.

[49] We have performed simulations with three different configurations for the drift velocity of the second electron beam. The simulation runs the with second beam injection presented different results, according to the relation between the first and second beam drift velocities. When $v_{db2} \geq v_{db1}$, the second injected beam is quickly modulated by the strong electrical field of previous Langmuir waves, which can be seen as a fast growth of electrical energy (see Figures 6a and 6c). The fast trailing beam particles release energy to waves generated by the leading beam at the initial stage of simulation. After a certain time, the slow leading beam particles absorb energy from the waves intensified by the trailing beam particles.

[50] In all cases where $v_{db2} \geq v_{db1}$, the harmonics are generated during the linear phase (vortex formation) and are intensified after this stage. These results are in accordance with a theory proposed by *Yoon et al.* [2003], according to which harmonics are generated during the linear phase. When we introduce the second beam with a drift velocity lower than that of the first beam, the harmonics are suppressed, because the particles are acquiring energy from the waves, as can be seen from Figure 6b.

[51] It is important to note that electromagnetic energy keeps growing for all cases with the second beam, independent of the second beam velocity. This result suggests that electromagnetic wave generation can be enhanced by

multiple electron beams injected in space plasmas and solar bursts. Our results suggest that a higher power waves observed can be obtained as a consequence of multiple electron beam interactions, as Figure 7 shows the continuous growth of electromagnetic energy after the second beam injection.

[52] Another new result found by including of the second electron beam was the bunching approximation of the harmonic electrostatic emission. Until now this downshift did not have an explanation. However, our simulation results suggest that the downshift is dependent on the second beam density. This will be addressed in a future paper.

[53] Both first and second electron beams are indistinguishable after a long time of the simulation run, forming just a single beam. This result is in agreement with the one obtained by *Li et al.* [2002]. We believe that the same would be true of the second case, had we run the simulation for a longer time.

[54] **Acknowledgments.** The authors would like to thank the Brazilian agencies Fundação de Amparo a Pesquisa do Estado de São Paulo (FAPESP) (project 2008/01288-0) and Conselho Nacional de Desenvolvimento Científico e Tecnológico (CNPq) (projects 474481/2007-7 and 304865/2007-9) for financial support.

[55] Amitava Bhattacharjee thanks the reviewers for their assistance in evaluating this paper.

References

Alves, M. V., A. C. L. Chian, M. A. E. de Moraes, J. R. Abalde, and F. B. Rizzato (2002), A theory of the fundamental plasma emission of type-III solar radio bursts, *Astron. Astrophys.*, *390*(1), 351–357.

Anderson, K. A., R. P. Lin, C. Gurgiolo, G. K. Parks, D. W. Potter, S. Werden, and H. Réme (1985), A component of nongyrotropic (phase-bunched) electrons upstream from the Earth's bow shock, *Phys. Fluids A*, *90*(11), 10,809–10,814.

Birdsall, C. K., and D. Fuss (1997), Clouds-in-clouds, clouds-in-cells physics for many-body simulation, *J. Comput. Phys.*, *135*(2), 141–148.

Birdsall, C. K., and A. B. Langdon (1991), *Plasma Physics via Computer Simulation*, 2nd ed., 479 pp., Inst. of Phys. Publ., Bristol, U. K.

Cairns, I. H. (1989), Electrostatic wave generation above and below the plasma frequency by electron-beams, *Phys. Fluids B*, *1*(1), 204–213.

Canu, P. (1989), Linear study of the beam-plasma interaction as a source mechanism for the broadband electrostatic emissions observed in the electron foreshock, *J. Geophys. Res.*, *94*(A7), 8793–8804.

Dum, C. T. (1990a), Simulation studies of plasma-waves in the electron foreshock: The generation of Langmuir waves by a gentle bump-on-tail electron-distribution, *J. Geophys. Res.*, *95*(A6), 8095–8110.

Dum, C. T. (1990b), Simulation studies of plasma-waves in the electron foreshock: The transition from reactive to kinetic instability, *J. Geophys. Res.*, *95*(A6), 8111–8122.

Gaelzer, R., P. H. Yoon, T. Umeda, Y. Omura, and H. Matsumoto (2003), Harmonic Langmuir waves: II. Turbulence spectrum, *Phys. Plasmas*, *10*(2), 373–381.

Ginzburg, V. L., and V. V. Zheleznyakov (1958), On the possible mechanism of sporadic solar radio emission (radiation in an isotropic plasma), *Sov. Astron. AJ USSR*, *2*, 653–668.

Gurnett, D. A., and A. Bhattacharjee (2004), *Introduction to Plasma Physics With Space and Laboratory Applications*, Cambridge Univ. Press, Cambridge, U. K.

Kasaba, Y., H. Matsumoto, and Y. Omura (2001), One- and two-dimensional simulations of electron beam instability: Generation of electrostatic and electromagnetic $2f_p$ waves, *J. Geophys. Res.*, *106*(A9), 18,693–18,711.

Li, B., P. A. Robinson, and I. H. Cairns (2002), Multiple electron beam propagation and Langmuir wave generation in plasmas, *Phys. Plasmas*, *9*(7), 2976–2987.

Li, B., A. J. Willes, P. A. Robinson, and I. H. Cairns (2005a), Second harmonic electromagnetic emission via beam-driven Langmuir waves, *Phys. Plasmas*, *1*(12), 012103, doi:10.1063/1.1812274.

Li, B., A. J. Willes, P. A. Robinson, and I. H. Cairns (2005b), Dynamics of fundamental electromagnetic emission via beam-driven Langmuir waves, *Phys. Plasmas*, *1*(12), 052324, doi:10.1063/1.1906214.

Matsumoto, H., and T. Sato (1985), *Computer Simulation of Space Plasmas*, 380 pp., Terra Sci., Tokyo.

Melrose, D. B. (1986), *Instabilities in Space and Laboratory Plasmas*, 280 pp., Cambridge Univ. Press, Cambridge, U. K.

Nishikawa, K. I., and I. H. Cairns (1991), Simulation of the nonlinear evolution of electron-plasma waves, *J. Geophys. Res.*, *96*(A11), 19,343–19,351.

Omura, Y., and H. Matsumoto (1993), Kempo1: Technical guide to one-dimensional electromagnetic particle code, in *Computer Space Plasma Physics: Simulation Techniques and Software*, edited by H. Matsumoto and Y. Omura, pp. 21–65, Terra Sci., Tokyo.

Robinson, P. A. (1997), Nonlinear wave collapse and strong turbulence, *Rev. Mod. Phys.*, *69*(2), 507–573.

Schriver, D., M. Ashour-Abdalla, V. Sotnikov, P. Hellinger, V. Fiala, R. Bingham, and A. Manganey (2000), Excitation of electron acoustic near the electron plasma frequency and at twice the plasma frequency, *J. Geophys. Res.*, *105*(A6), 12,919–12,927.

Simões Junior, F. J. R. (2008), Computational Simulation of electromagnetic emission in space plasmas, Ph.D. thesis, 163 pp., Inst. Nac. de Pesqui. Espaciais, São José dos Campos.

Simões Junior, F. J. R., M. V. Alves, and F. B. Rizzato (2005), Energy mode distribution: an analysis of the ratio of anti-stokes to stokes amplitudes generated by a pair of counterpropagating langmuir waves, *J. Atmos. Sol. Terr. Phys.*, *67*, 1680–1686.

Sotnikov, V. I., V. Fiala, P. M. E. Décréau, V. V. Pivovarov, and I. V. Shapiro (1994), Contribution to the nonlinear theory of plasma wave excitation inside the electron foreshock region, *J. Geophys. Res.*, *99*(A12), 23,473–23,479.

Umeda, T., Y. Omura, P. H. Yoon, R. Gaelzer, and H. Matsumoto (2003), Harmonic Langmuir waves: III. Vlasov simulation, *Phys. Plasmas*, *10*(2), 382–392.

Yoon, P. H. (2000), Generalized weak turbulence theory, *Phys. Plasmas*, *7*(12), 4858–4871.

Yoon, P. H., and R. Gaelzer (2002a), Effects of nonlinear frequency shifts on certain induced scattering processes, *Phys. Plasmas*, *9*(11), 4520–4524.

Yoon, P. H., and R. Gaelzer (2002b), Nonlinear frequency shifts of plasma eigenmodes, *Phys. Plasmas*, *9*(10), 4166–4173.

Yoon, P. H., R. Gaelzer, T. Umeda, Y. Omura, and H. Matsumoto (2003), Harmonic Langmuir waves: I. Nonlinear dispersion relation, *Phys. Plasmas*, *10*(2), 364–372.

Zakharov, V. E. (1984), Collapse and self-focusing of Langmuir waves, in *Handbook of Plasma Physics*, edited by A. A. Galeev and R. N. Sudan, chap. 5.3, pp. 81–121, North-Holland, Amsterdam.

M. V. Alves, Laboratório Associado de Plasmas, Instituto Nacional de Pesquisas Espaciais, Av. dos Astronautas 1758, Jardim da Granja, 12227-010, São José dos Campos, SP, Brazil.

R. Gaelzer and F. J. R. Simões Jr., Instituto de Física e Matemática, Universidade Federal de Pelotas, Rua Gomes Carneiro 1, Centro, CEP 96010-610, Pelotas, RS, Brazil. (fernando@plasma.inpe.br)